Materials Letters 64 (2010) 207–210

Contents lists available at ScienceDirect

Materials Letters

journal homepage: www.elsevier.com/locate/matlet

Nanoindentation and microstructure analysis of resistance spot welded dual phase steel

V.H. Baltazar Hernandez [a,b,*], S.K. Panda [a,c,1], M.L. Kuntz [a,2], Y. Zhou [a,3]

[a] Centre for Advanced Materials Joining, University of Waterloo, Waterloo, Ontario, Canada
[b] MPyM-EPMM Academic Unit of Engineering, Autonomous University of Zacatecas, Mexico
[c] Mechanical Engineering Department, Indian Institute of Technology Kharagpur, India

ARTICLE INFO

Article history:
Received 30 March 2009
Accepted 16 October 2009
Available online 24 October 2009

Keywords:
Tempering
Nanoindentation
Dual phase steel
Hardness
Rapid thermal cycles

ABSTRACT

A nanoindentation hardness study has been conducted on the tempered region and the base metal in a dual phase steel subjected to rapid thermal cycles of resistance spot welding. Nanohardness results revealed "softening" at nano-scale for tempered martensite when compared to martensite in the base metal. At the tempered region, the ferritic matrix presented a slight reduction in hardness while the tempered martensite seemed to have a major contribution to the measured softening at micro-scale.

© 2009 Elsevier B.V. All rights reserved.

1. Introduction

Dual phase (DP) composed of ferrite matrix and martensite particles is part of the family of advanced high strength steels (AHSS) that offers improved mechanical properties (i.e. increased ultimate strength along with good ductility) making it suitable for automotive applications [1].

Reduction in Vickers micro-hardness has been observed in DP steel when subjected to rapid thermal cycles during laser and/or resistance spot welding. This is referred to as heat affected zone (HAZ) softening in the literature [2–4]. Tempering of martensite has been documented as the main cause of softening in martensitic steels, and the degree of tempering has been extensively studied through traditional micro-hardness testing [5–7]. Few studies of tempering have so far been attempted using instrumented nanoindentation techniques. For instance, fully martensitic steels were held at tempering temperature for extended periods of time of up to 5400 s; nanoindentations were made on tempered martensite and the effect of grain boundaries on the nanohardness was discussed [8]. A martensitic Fe–C steel was tempered by typical heat treatment at various peak temperatures; the relation between nanohardness through Berkovich indentation and Vickers micro-hardness was discussed for decomposed martensite [9]. However, no studies have been addressed to evaluate the hardness at nano-scale of individual micro-constituents in the tempered region of dual phase steel under conditions of fast heating, very short time at peak temperature, and very rapid cooling.

This work aims to evaluate the nanohardness characteristics of individual phases in the tempered region and the unaffected base metal of dual phase steel subjected to rapid sub-critical thermal cycles in resistance spot welding.

2. Experimental

DP steel with a nominal strength of 980 MPa and martensite volume fraction of 48% was used in the present study. The main alloying elements were: 0.13-C, 1.90-Mn, 0.03-Si, 0.16-Cr, and 0.33-Mo. The steel was resistance spot welded using previously optimized welding parameters [10]. Welding conditions such electrode stabilization, coupon dimensions, etc., were adjusted according to AWS standards [11]. The region affected by the heat outside the melted zone was observed under the optical microscope to be conveniently subdivided at the Ac_1 line of critical temperature [7] as: heat affected zone (HAZ) above Ac_1, and sub-critical-HAZ below Ac_1 temperature. Calculated transformation temperature at Ac_1 was 726.4 °C [12]. The thermal history within the sub-critical heat affected zone was evaluated through commercial numerical simulation software in which a heating rate of 1250 °C/s and a cooling rate of 1500 °C/s were estimated. The simulated thermal cycle agreed well with referenced work [13].

Samples for scanning electron microscopy (SEM) observations were prepared by conventional metallographic techniques. Vickers micro-

* Corresponding author. Centre for Advanced Materials Joining, University of Waterloo, Waterloo, Ontario, Canada. Tel.: +1 519 8884567x35256; fax: +1 519 8884351.
E-mail addresses: v.h.baltazar@gmail.com (V.H. Baltazar Hernandez), sushanta.panda@gmail.com (S.K. Panda), mlkuntz@engmail.uwaterloo.ca (M.L. Kuntz), nzhou@mecheng1.uwaterloo.ca (Y. Zhou).
[1] Tel.: +91 3222 282910.
[2] Tel.: +1 519 8884567x37303.
[3] Tel.: +1 519 8884567x36095.

0167-577X/$ – see front matter © 2009 Elsevier B.V. All rights reserved.
doi:10.1016/j.matlet.2009.10.040

hardness (HV) indentations were performed using an indenter load of 200 g for a period of 15 s and the indentations were spaced 200 μm apart.

Nanoindentation was performed in a Hysitron triboindenter TI-900 equipped with a scanning probe microscope (SPM) for imaging. The Berkovich nanoindenter was calibrated by using a reference specimen of fused silica. A loading–unloading period of 20 s was programmed. After performing several trials at different load conditions, a constant load of 3000 μN was established. Specimens were nanoindented for several surface conditions (i.e. mechanically fine polished, deep etched, and electropolished) and it was found that systematic variations in nanohardness of constituents were insignificant. A minimum number of 49 indentations were performed on each assessed region for reproducibility.

3. Results and discussion

Fig. 1(a) shows a micro-hardness profile obtained across the welded region from the unaffected base metal (BM) through the fusion zone (FZ). A reduction in hardness (softening) with respect to BM (avg. 298 HV) was clearly revealed in the sub-critical HAZ. The width of the zone of significant softening was around 0.8 mm and a maximum hardness reduction of 40 HV was identified at location C. Maximum softening (at C) was located just below the line of critical temperature Ac_1. The location of Ac_1 was determined experimentally through optical microscopy by analysing the cross section macrostructure of the welded region. Detailed procedures for identification of Ac_1 have been explained elsewhere [2]. During the welding thermal cycle, transient peak temperatures above Ac_1 mean, by definition, that the martensite and part of the ferrite is briefly transformed to austenite and then retransformed to new martensite during cooling. Depending on the location within the HAZ and hence on the peak temperature reached, the local post-weld martensite content could be above the level in the as-manufactured steel, leading to higher local hardness [14]. The RSW cross section macrostructure along with the micro-hardness indentations have been detailed in previous work [10].

The SEM image provided in Fig. 1(b) depicts the un-tempered (BM) microstructure which corresponds to the point B in Fig. 1(a). Solid martensite islands (grey coloured particles) were clearly embedded in the ferrite matrix (black area). Martensitic particles were preferentially situated at the prior austenite grain boundaries [15]. The microstructure in Fig. 1(c) which was obtained at the sub-critical HAZ, revealed decomposition of martensite particles (tempered martensite), and corresponds to location C in Fig. 1(a). The morphology of the tempered martensite appeared broken with presence of some submicron particles (white), presumably due to precipitation and coarsening of cementite carbides and recovery of martensite [6,7].

It is clear from Fig. 1(a) that measured softening is associated with the martensite tempering depicted in Fig. 1(c). A single Vickers micro-hardness impression size ranged from 35 to 39 μm on the tempered region (TR) [16]. The scale of Fig. 1(c) indicated that a single indentation covered several phase grains, but evidence of the contribution of individual phases to softening was unclear. The nanoindentation trials were therefore specifically designed to investigate tempering-induced effects on individual phases. Tests were carried on two specific locations: base metal (at B) and tempered region (at C) with reference to Fig. 1(a).

Typical load progression (load-displacement or *P–h)* curves during nanoindentation of the base metal and tempered region are shown in Fig. 2. SEM micrographs of representative Berkovich impressions for BM and TR are shown in Fig. 3 and these impressions correspond to the *P–h* curves plotted in Fig. 2.

Referring to the *P–h* curves for martensite and tempered martensite in Fig. 2(a), the slope of the curves kept on increasing

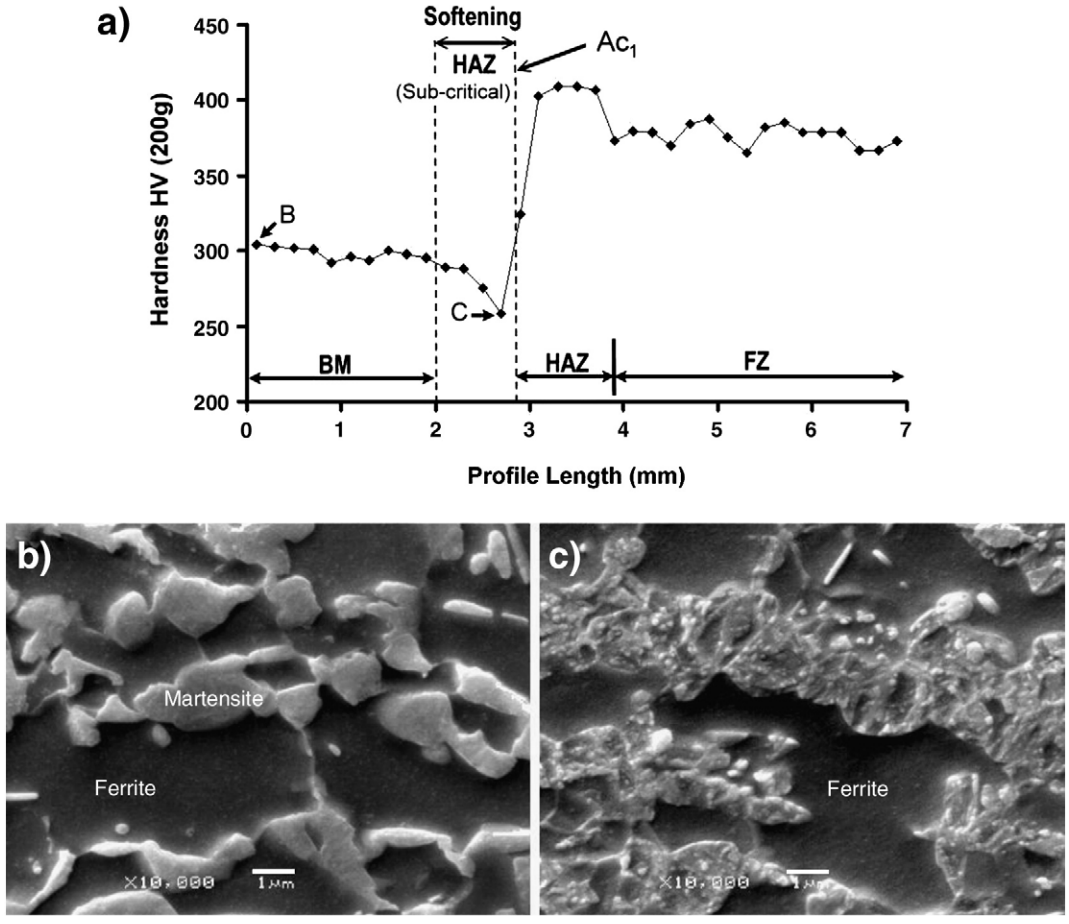

Fig. 1. (a) Vickers micro-hardness indentation profile across the weld, (b–c) SEM micrographs for base metal (BM) and the sub-critical region (HAZ) respectively.

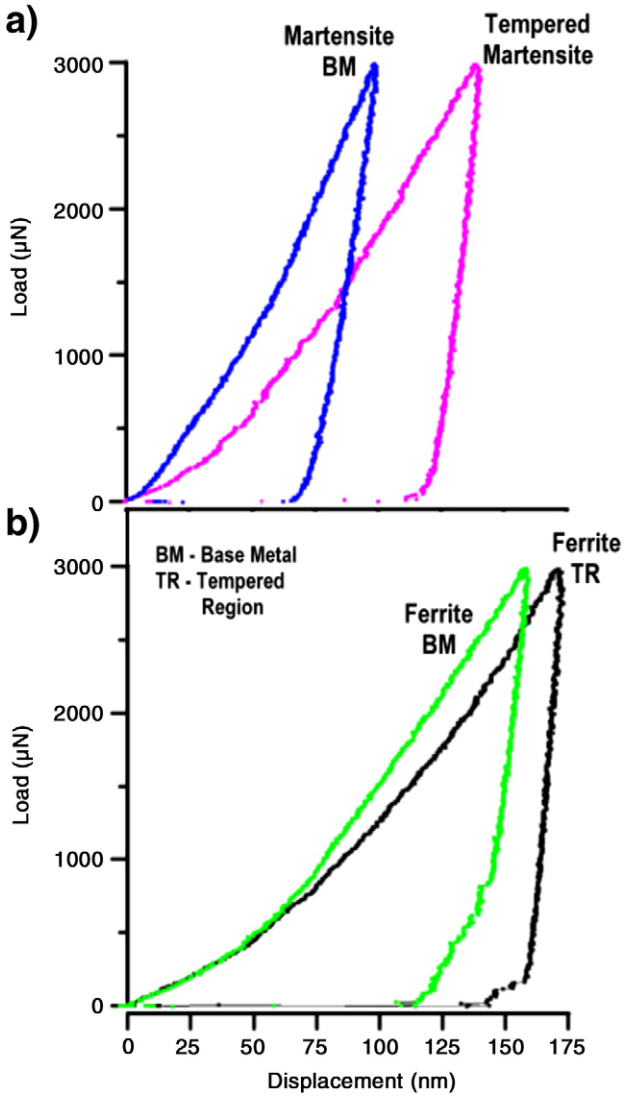

Fig. 2. Un-tempered (BM) and tempered region (TR) load-displacement curves (P–h) corresponding to: (a) martensite and tempered martensite and, (b) ferrite.

due to increase in contact area during indentation. The maximal indenter displacement (h_{max}) upon a peak load of 3000 μN was larger for tempered martensite (i.e. 140 nm) compared to that of BM-martensite (99 nm). Larger penetration depth was also obtained for ferrite at the tempered region compared to that of the base metal (Fig. 2b). Maximum penetration depth values for tempered martensite were in between the h_{max} values for BM-ferrite and BM-martensite.

Pop-in behaviour is known as a sudden or abrupt jump in displacement of the indenter associated to large-scale dislocation nucleation at the onset of plastic deformation and it is a function of pre-existing dislocation density [17]. Pop-in has been reported for tempered martensite in Fe–C alloys heat treated below Ac_1 temperature (500 °C and 650 °C) for prolonged periods of time (i.e. 5400 s) in which a considerable reduction of dislocation density by recovery was assumed [18]. It should be noticed that the above mentioned heat treatment is associated to traditional isothermal time–temperature processes well described by the Hollomon–Jaffe tempering parameter [19]. In contrast, for the non-isothermal condition, continuous deformation without pop-in behaviour was observed for tempered martensite during the loading stage suggesting partial tempering of martensite, this is presumed to be due to low rate of carbide precipitation and incomplete recovery as observed by SEM micrographs (i.e. Fig. 1c). Partial tempering encountered in HAZs of this RSW-DP steel can be attributed to the rapid thermal cycles of heating and cooling (short hold time at the peak temperature),[20,21] and, to the relatively high concentration of Mn in the alloy that retards the coalescence of carbides and the grain growth of ferrite [5,6].

Single indentations made on the un-tempered region for martensite and ferrite are illustrated in Fig. 3a, and Fig. 3b respectively. The size (depth–width) of the nanoindenter impressions appeared appropriate for hardness assessment of individual phases as the measured indentations were located within the area of martensite particles (Fig. 3a), thus avoiding contributions of grain boundaries between phases to nanohardness.

Pile-up or excursion, defined as plastically flowed material deposited at the perimeter of the indentation [22], was barely observed in martensite as shown in Fig. 3a. By noting the minimal pile-up effect for martensite it can be inferred that nanohardness for this phase was not overestimated [23]. Fig. 3b illustrates the topography of a typical indent on the untempered ferrite matrix showing some deformation of the surroundings. Fig. 3c shows a typical indent located within the boundaries of decomposed (tempered) martensite, showing that the measured nanohardness of the tempered martensite represents all the transformed sub-products such as carbides and/or partial recrystallized zones. The impressions on ferrite at the tempered region in Fig. 3d resulted in the largest pile-up at the periphery of the indent in comparison to other phases (i.e., martensite). In addition, calculation of h_f/h_{max} yielded a value of 0.85 (where h_f is the final displacement after complete unloading): when this value is higher than 0.7 it suggests pile-up for ferrite at TR [24].

The averaged nanohardness for the tempered and the un-tempered (BM) regions shown in Fig. 4 clearly revealed martensite to be the harder constituent (i.e., approximately 7.5 GPa). Tempered martensite (TM) hardness was about 4 GPa, which lay between the hardness values for martensite and ferrite. Nanohardness for martensite and ferrite for advanced high strength steel has been little reported in literature. For instance, Chen et al. [25] nanoindented a welded region in a 780 MPa Al-TRIP steel: the hardness of martensite was 5.5 GPa whereas allotriomorphic ferrite ranged from 2.6 to 3.1 GPa. Even though results for ferrite in this work appeared consistent with those reported in literature as they lay in approximately the same range, still, a base of comparison for nanohardness values of multiphase steels appears premature mainly due to local variations of chemistry for individual constituents as well as the prior thermal history.

Significant nanohardness reduction of the decomposed martensite revealed “softening” at nano-scale in dual phase steel. It is evident that tempered martensite contributes the most to the measured softening at micro-scale (point C in Fig. 1a), however, a small contribution can also be expected from the ferrite matrix as it also showed a slight reduction in nanohardness at the tempered region as indicated by Fig. 4. Nanohardness reduction in the ferrite phase can be attributed to a possible reduction in the dislocation density [16].

Detailed transmission electron microscopy needs to be explored in order to better understand martensite decomposition; however, the above results indicate that the instrumented nanoindentation technique is useful to study tempering kinetics of martensite under varied thermal cycling.

4. Conclusions

A nanoindentation hardness study was successfully conducted on the base metal and tempered region of a dual phase steel subjected to a rapid thermal cycle in resistance spot welding. Tempered martensite resulted in a significant reduction in nanohardness with respect to martensitic particles in the base metal. It was found that the decomposed martensite was the major contributor to “measured” softening at micro-scale. Ferrite in the sub-critical HAZ was also observed to have a minor reduction in nanohardness. Nanoindentation results showed continuous deformation during the loading stage for

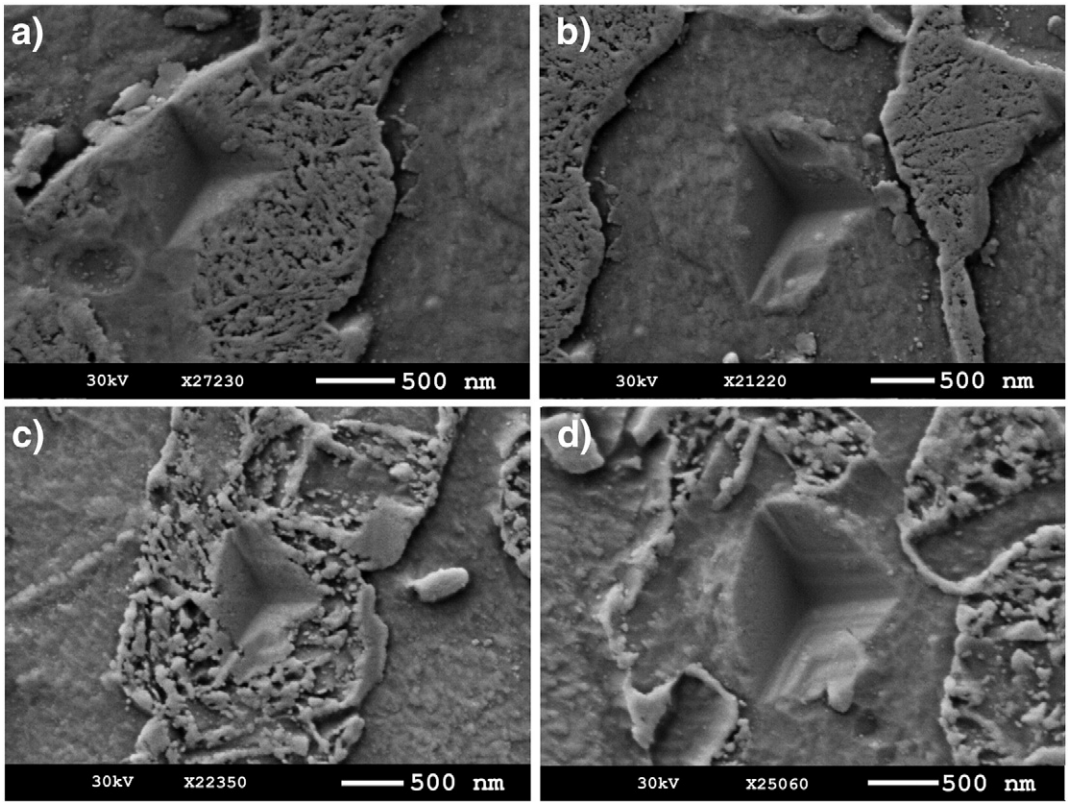

Fig. 3. Hardness nanoindentation impressions on: BM at (a) martensite, (b) ferrite, and, TR at (c) tempered martensite (d) ferrite.

tempered martensite in this work, which contrast the pop-in behaviour for tempered martensite when subjected to extended heat treatment duration.

Acknowledgments

The authors would like to acknowledge the funding from Auto21, one of the Networks of Centres for Excellence supported by the Canadian Government, The Initiative for Automotive Manufacturing Innovation (IAMI) supported by the Ontario Government, International Zinc Association (IZA), Belgium, and Arcelor Mittal Dofasco and Huys Industries in Canada. V.H. Baltazar Hernandez would also like to acknowledge the support from CONACYT Mexico and the Autonomous University of Zacatecas Mexico. The author would also like to acknowledge the comments and suggestions of Prof Scott Lawson from the Centre for Advanced Materials Joining at University of Waterloo.

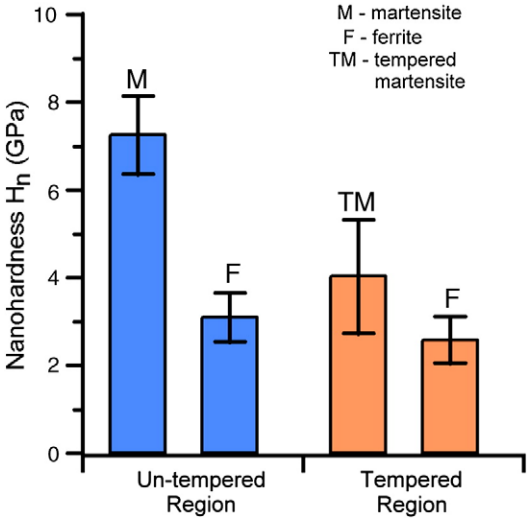

Fig. 4. Nanohardness characteristics for several phases at two locations.

References

[1] Committee on Automotive Applications: AHSS - application guidelines, vol. 3. International Iron and Steel Institute; 2006. p. 1–4.
[2] Xia M, Biro E, Tian Z, Zhou Y. ISIJ Int 2008;48:809.
[3] Marya M, Wang K, Hector LG, Gayden X. J Manuf Sci Technol 2006;128:287.
[4] Panda SK, Sreenivassan N, Kuntz ML, Zhou Y. J Eng Mater Tech 2008;130:041003.
[5] Grange RA, Hribal CR, Porter LF. Metall Trans 1977;8A:1775.
[6] Speich GR, Leslie WC. Metall Trans 1972;3:1043.
[7] Honeycombe RWK, Bhadeshia HKDH. Steels—microstructure and properties. sec. ed. Great Britain: Arnold; 1981.
[8] Ohmura T, Hara T, Tsuzaki K. Scr Mater 2003;49:1157.
[9] Ohmura T, Tsuzaki K, Matsuoka S. Philos Maga 2002;82–10:1903.
[10] Baltazar Hernandez VH, Kuntz ML, Khan MI, Zhou Y. Sci Technol Weld Join 2008;13:769.
[11] ANSI/AWS/SAE/D8.9–97. Recommended practices for test methods for evaluating the resistance spot welding behavior of automotive steels; 1997.
[12] N. Yurioka: Weldability calculation, http://homepage3.nifty.com/yurioka/exp.html. Accessed November 18 2008.
[13] I. Khan, M.L. Kuntz, Y. Zhou, K. Chan, N. Scotchmer, SAE, Tech. P. (2007)-01-1370.
[14] Easterling K. Introduction to the physical metallurgy of welding. Butterworths; 1983.
[15] Chowdhury SG, Pereloma EV, Santos DB. Mater Sci Eng A 2008;480:540.
[16] Panda SK, Baltazar Hernandez VH, Kuntz ML, Zhou Y. Metall Mater Trans A 2009;40-8:1955.
[17] Zbib AA, Bahr DF. Metall Mater Trans A 2007;38:2249.
[18] Ohmura T, Hara T, Tsuzaki K, Nakatsu H, Tamura Y. J Mater Res 2004;19-1:79.
[19] Hollomon JH, Jaffe LD. Trans AIME 1945;162:223.
[20] Furuhara T, Kobayashi K, Maki T. ISIJ Int 2004;44-11:1937.
[21] Doane DV, Kirkaldy JS. Hardenability concepts with applications to steel. Warrendale, PA: American Institute of Mining, Metallurgical and Petroleum Eng; 1978. p. 250.
[22] Kese KO, Li ZC, Bergman B. Mater Sci Eng A 2005;404:1–8.
[23] Oliver WC, Pharr GM. J Mater Res 2004;19-1:3.
[24] Bolshakov A, Pharr GM. J Mater Res 1998;13-4:1049.
[25] Chen J, Sand K, Xia MS, Ophus C, Mohammadi R, Kuntz ML, et al. Metall Mater Trans A 2008;39:593.